



SPE 149094

Use of the Memory Concept to Investigate the Temperature Profile during a Thermal EOR Process

M. Enamul Hossain, SPE, Sidqi A. Abu-Khamsin, SPE, King Fahd University of Petroleum & Minerals and Abdul-Aziz Al-Helali, King Fahd University of Petroleum & Minerals

Copyright 2011, Society of Petroleum Engineers

This paper was prepared for presentation at the 2011 SPE Saudi Arabia Section Technical Symposium and Exhibition held in AlKhobar, Saudi Arabia, 15–18 May 2011.

This paper was selected for presentation by an SPE program committee following review of information contained in an abstract submitted by the author(s). Contents of the paper have not been reviewed by the Society of Petroleum Engineers and are subject to correction by the author(s). The material, as presented, does not necessarily reflect any position of the Society of Petroleum Engineers, its officers, or members. Papers presented at the SPE meetings are subject to publication review by Editorial Committee of Society of Petroleum Engineers. Electronic reproduction, distribution, or storage of any part of this paper without the written consent of the Society of Petroleum Engineers is prohibited. Permission to reproduce in print is restricted to an abstract of not more than 300 words; illustrations may not be copied. The abstract must contain conspicuous acknowledgment of where and whom the paper was presented. Write Librarian, SPE, P.O. Box 833836, Richardson, TX 75083-3836, U.S.A., fax 01-972-952-9435.

Abstract

Accurate prediction of the temperature profile within a reservoir undergoing a thermal recovery process is a key factor in process design, production forecasting and reservoir management. Such profile is governed by the heat transfer between the rock matrix and flowing fluids, which is highly dependent on the thermal and rheological properties of the rock and fluids involved. In this work, the role of temperature-dependent rock and fluid properties in the development of the temperature profile during the thermal process was investigated employing the continuous time function as “memory.” Mathematical models were developed in terms of a group of heat transfer dimensionless numbers that correlate the varying rock and fluid properties. New heat transfer dimensionless numbers are proposed which can be characterized by rock and fluid properties. The model equations were then solved numerically through MATLAB programming to produce temperature profiles for a typical steam flood where the rock and fluid temperatures are assumed unequal throughout the reservoir, i.e. the rock does not attain the fluid temperature instantaneously. Results reveal the development of a temperature profile within the growing condensed water zone that is flowing ahead of the steam zone. The rock and fluid temperature profiles were found sensitive to the rheological properties, time and fluid velocity. The proposed model would be useful for better prediction of reservoir performance.

Keywords: porous media, dimensionless number, temperature distribution, temperature profile, reservoir modeling, reservoir management, heat transfer coefficient

INTRODUCTION

Production decline from mature reservoirs is a major concern for the petroleum industry. Thermal flooding, which involves the injection of hot water or steam into the reservoir, is an enhanced oil recovery technique that has proven effective in prolonging production from many reservoirs worldwide. Many wells produce hydrocarbons at a high water/oil ratio due to water coning and fingering. In such a situation, economic production is compromised by producing below the critical flow rate to avoid water breakthrough [1]. A thermal operation may be effective in improving the oil mobility and, thus, increasing production rates.

Thermal EOR process is widely used for decades in enhancing hydrocarbon recovery. Figure 1 shows a typical thermal recovery process where upstream and downstream equipment and facilities are shown which has been demonstrated by Hossain et al. [2 – 3] and several other authors [4 – 6]. In steam flooding, where steam is injected into a number of wells while the oil is produced from adjacent wells (Figure 1), alterations of rock and fluid properties guide the temperature profile within the reservoir formation. Proper analysis of temperature propagation within the formation may help forecast performance parameters of the flood, which improves reservoir management. It can also be an effective diagnostic tool to identify potential problems such as water or gas encroachment or fingering, early breakthrough, open fractures, and inter-layer communication. It is also important in guiding the action of sliding sleeves and other downhole flow control devices. Therefore, it is useful to investigate the pattern of temperature propagation and heat exchange between fluid and rock in the formation.

Corresponding author: Dr. M. Enamul Hossain, Department of Petroleum Engineering, P.O. Box 2020, King Fahd University of Petroleum & Minerals (KFUPM), Dhahran 31261, Saudi Arabia. Tel: 0096638602305, Fax: 0096638604447, Email: menamul@kfupm.edu.sa; dr.mehossain@gmail.com

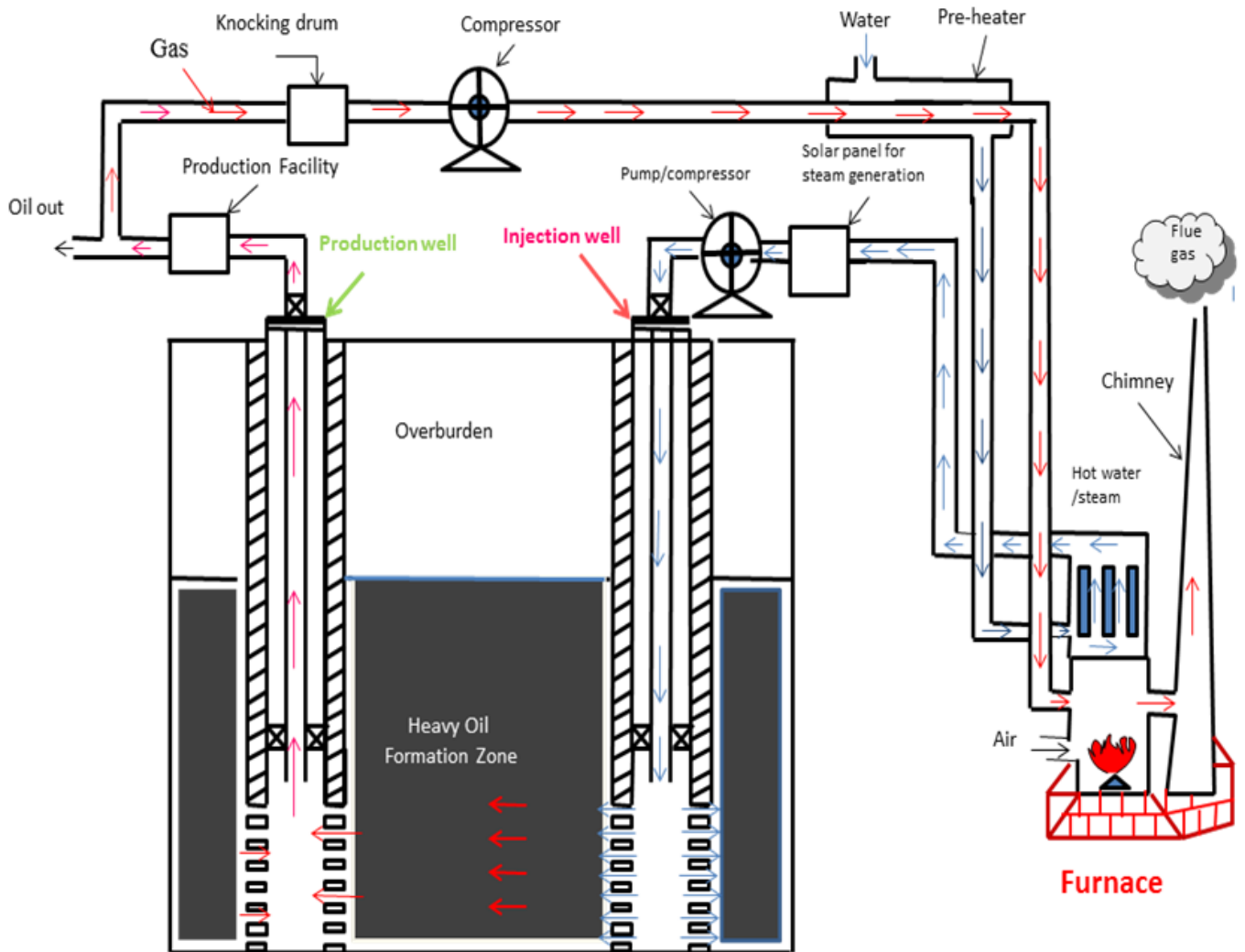


Figure 1. Mechanism of a sustainable thermal oil recovery scheme in a heavy oil reservoir (redrawn from Hossain et al. [3])

The use of temperature profile in a horizontal well for detecting water entry has been previously attempted by several authors [3, 7, 8]. Assuming equal temperatures for the flowing fluid and rock, they varied the production rate and types of oil to see their effects on the temperature profile. However, they did not check the effects of fluid velocity and injection steam velocity on temperature distribution. Hossain et al. [3, 9] investigated the influence of fluid and injection steam velocity and showed the variation of the temperature profile if the rock and fluid temperatures are assumed different. An extensive review of temperature propagation and its dependence on several parameters was presented by Hossain et al. [3, 9 – 10]. Yoshioka et al. [11, 12] presented models for predicting the temperature profile in a horizontal well. They presented methods [11] to interpret measurements in complex wells for determining the inflow profiles of oil, gas and water under steady-state flow conditions. They considered a box-shaped homogeneous reservoir and assumed each segment to be ideally isolated. They investigated the effects of production rate, permeability and fluid types on temperature profiles.

During steam injection of an EOR scheme, alterations of rock and fluid properties are well established in the literature especially by Hossain et al., [2, 13, 14]. Such alteration guides the temperature profile within the reservoir formation which provides information on the water influx in the permeable zone. Therefore, understanding the temperature propagation is important in the process design and management.

Spillette's model [15] is based on the assumption that heat transfer within the reservoir takes place by two mechanisms: 1) the physical movement of the injected fluids and 2) thermal conduction. Convective heat transfer between the injected fluid and the original reservoir fluids and the permeable reservoir rock is assumed to be accounted for by the additional assumption of instantaneous thermal equilibrium in the reservoir. Hossain et al. [2, 3, 9] investigated temperature propagation pattern and its dependence on various parameters during thermal operations. They have completed an extensive review of temperature propagation and its dependence on several parameters. The model equations have been solved for temperature distribution throughout the reservoir for different cases. Results show that formation fluid velocity, steam injection velocity, and time have an impact on the behavior of temperature profiles. They identified that temperature distribution is much more sensitive to time,

and formation fluid velocity. It is also sensitive to steam or hot water injection rate or velocity. They assumed a linear function for fluid velocity in the formation. They did not consider the thermal effects in terms of Nusselt number, Peclet number and Prandtl number. Further investigation shows that due to temperature variation in the formation, the porosity, permeability and the rheology of reservoir may also change as a result of continuous heat transfer within the fluid and rock matrix [10, 13, 14]. This continuous alteration of fluid and pore space properties may greatly be influenced by the fluid memory especially in some geothermal area [10, 13, 14].

Therefore, the present study includes the effects of fluid memory in the fluid flow behavior during steam injection into an oil reservoir. As the literature shows that the fluid velocity, and time have strong effects on temperature propagation pattern, it is very important to investigate the effects of fluid memory as well as the rheology of rock/fluid based on heat transfer. In this study we are focusing how to model the complex heat transfer phenomena and alteration of temperature between rock and fluid and its influence on temperature profile in terms of Nusselt number, Peclet number and Prandtl number and two proposed numbers [16]. The existing models are unable to handle the alteration rock/fluid properties with time during thermal operation. So, the main objective of this study is to develop mathematical models to address this issue. The model equations are solved using Matlab coding to analyze the temperature profiles which is sensitive to time dimension. This analysis will give advance information on any change or anomaly of temperature profile due to water entry or breakthrough.

MODEL DESCRIPTION

It is taken into account a porous medium of uniform cross sectional area and homogeneous along the x -axis. It is normal practice to consider fluid flow in porous media to be governed by Darcy's law. Since the medium is homogeneous, the pressure along the x -direction can be considered to vary initially according to Darcy diffusivity equation. In this study, we have used the modified Darcy's law, which represents the notion of fluid memory. It is also considered that the thermal conductivities of both the fluid and solid rock matrix are not functions of temperature and, thus, are constant along the medium. Before initiation of the flood, both pressure and temperature are uniformly distributed throughout the reservoir. The initial and boundary conditions are defined as:

$$T_f(x, 0) = T_s(x, 0) = T_i, T_f(0, t) = T_s(0, t) = T_{st}, \text{ and } T_f(L, t) = T_s(L, t) = T_i \quad (1)$$

MATHEMATICAL FORMULATION OF THE MODEL

To determine the temperature distribution in space and time, the energy balance equation is applied to both rock and fluid separately. The partial differential equations have a familiar form because the system has been averaged over representative elementary volumes (REV). A right-handed Cartesian coordinate system is utilized where the x -axis is along the formation length. The mass flow rate and conservation of energy equations are employed in developing the model for temperature distribution in porous media.

For an incompressible fluid and 1D horizontal reservoir, the fluid velocity through the porous medium can be written using the continuity and momentum balance equations for describing the motion of a fluid phase through the system [2, 17 – 18]. However, the inclusion of time-dependent rock and fluid properties is of great significance to reservoir engineers because the most uncertain parameter is accurate prediction of production performance [2, 13, 19]. Therefore, consideration of time-dependent phenomena is very important for a well managed recovery project. To introduce the notion of time dependency in temperature distribution, the use of "memory" concept is a recent and well established tool [2, 13, 19 – 21]. With the inclusion of "memory" concept, the modified Darcy's law is introduced as a rigorous flow rate equation, which may be written as [22]:

$$u_m = - \frac{\eta}{\Gamma(1-\alpha)} \int_0^t (t - \xi)^{-\alpha} \left[\frac{\partial^2 p}{\partial \xi^2 \partial x} \right] \partial \xi \quad \text{with } 0 \leq \alpha < 1. \quad (1)$$

The notation u_m is the fluid velocity, which represents time dependency and includes memory. Hossain et al. [19] defined the composite variable, η , which is a function of permeability and viscosity for any type of reservoir as:

$$\eta = \frac{k}{\mu_{ob}} (t)^\alpha \quad (2a)$$

For a sandstone reservoir, Hossain et al. [22] employed the composite variable, η as:

$$\eta = \frac{[3.0 (p/6894.76)^{-0.31+10.5}] \times 10^{-12}}{\mu_{ob} e^{8.422 \times 10^{-5}(p-p_b)}} (t)^\alpha \quad (2b)$$

where,

$$\mu_{ob} = 6.59927 \times 10^5 R_s^{-0.597627} T^{-0.941624} \gamma_g^{-0.555208} API^{-1.487449}$$

$$p_b = -620.592 + 6.23087 \frac{R_s \gamma_o}{\gamma_g B_o^{1.38559}} + 2.89868 T$$

$$B_o = B_{ob} e^{-C_o(p-p_b)}$$

$$B_{ob} = 1.122018 + 1.410 \times 10^{-6} \frac{R_s T}{\gamma_o^2}$$

$$C_o = (-70603.2 + 98.404 R_s + 378.266 T - 6102.03 \gamma_g + 755.345 API)/(p + 3755.53)$$

Equation (2b) is based on oil field units which are: oil formation volume factor (B_o), rb/stb; oil compressibility (C_o), psi^{-1} ; oil formation volume factor at the bubble point (B_{ob}), rb/stb; oil viscosity at the bubble point (μ_{ob}), cp; oil viscosity above the bubble point (μ_{ab}), cp; solution gas oil ratio (R_s), scf/stb ; crude oil temperature (T), °F; gas specific gravity (γ_g), lb_m/ft^3 ; oil specific gravity (γ_o), lb_m/ft^3 ; and oil API gravity (API), °API.

To develop a model equation for describing the temperature propagation in porous media, a 1D energy balance equations can be written [2, 9, 23] as:

$$k_s \frac{\partial^2 T_s}{\partial x^2} = (1 - \phi) \rho_s c_{ps} \frac{\partial T_s}{\partial t} + \frac{h_c}{L} (T_s - T_f) \quad (3)$$

$$k_f \frac{\partial^2 T_f}{\partial x^2} - \rho_f c_{pf} u_x \frac{\partial T_f}{\partial x} = \phi \rho_f c_{pf} \frac{\partial T_f}{\partial t} + \frac{h_c}{L} (T_f - T_s) \quad (4)$$

where,

$$c_{pf} = c_{pw} S_w + c_{po} S_o + c_{pg} S_g \quad (5)$$

$$\rho_f c_{pf} = \rho_w c_{pw} S_w + \rho_o c_{po} S_o + \rho_g c_{pg} S_g \quad (6)$$

$$k_f = k_w S_w + k_o S_o + k_g S_g \quad (7)$$

$$k_e = \phi k_f + (1 - \phi) k_s \quad (8)$$

$$\rho_f = \rho_w S_w + \rho_o S_o + \rho_g S_g \quad (9)$$

$$S_w + S_o + S_g = 1 \quad (10)$$

$$M = (1 - \phi) \rho_s c_{ps} + \phi \rho_w c_{pw} S_w + \phi \rho_o c_{po} S_o + \phi \rho_g c_{pg} S_g \quad (11)$$

Equations (3) and (4) represent the governing energy balance equations when both rock and fluid temperatures are considered separately and are not equal (i.e. $T_s \neq T_f$). These two equations can be transformed into dimensionless forms using the non-dimensional parameters defined as: $T^* = \frac{T}{T_i}$, $T_s^* = \frac{T_s}{T_i}$, $T_f^* = \frac{T_f}{T_i}$, $x^* = \frac{x}{L}$, $p^* = \frac{p}{p_i}$, $q^* = \frac{q_{prod}}{q_i}$, $t^* = \frac{k t}{\phi \mu c_t L^2}$, $\xi^* = \frac{k \xi}{\phi \mu c_t L^2}$ where L is the distance between the production and injection wells. Substituting the above transformations into Eq. (3) yields:

$$k_s \frac{T_i}{L^2} \frac{\partial^2 T_s^*}{\partial x^{*2}} = (1 - \phi) \rho_s c_{ps} \frac{T_i k}{\phi \mu c_t L^2} \frac{\partial T_s^*}{\partial t^*} + \frac{h_c}{L} (T_s^* T_i - T_f^* T_i) \quad (12)$$

Equation (12) reduces to:

$$\left\{ \frac{(1-\phi) \rho_s c_{ps}}{\phi} \right\} \times \left\{ \frac{\mu c_{pf}}{k_e} \right\} \frac{\rho_f k}{\mu \mu c_t} \frac{L_c}{L} \frac{\partial T_s^*}{\partial t^*} - \frac{k_s L_c}{k_e L} \frac{\partial^2 T_s^*}{\partial x^{*2}} + N_{NuL} (T_s^* - T_f^*) = 0 \quad (13)$$

The final form of Eq. (13) is, thus, written as:

$$N_{HA1} N_{Pr} N_{HA2} \frac{\partial T_s^*}{\partial t^*} - \frac{k_s}{k_e} \frac{\partial^2 T_s^*}{\partial x^{*2}} + N_{NuL} \frac{L}{L_c} (T_s^* - T_f^*) = 0 \quad (14)$$

where

$$N_{HA1} = \frac{k \rho_f}{\mu^2 c_t}, \text{ and } N_{HA2} = \frac{(1-\phi) \rho_s c_{ps}}{\phi \rho_f c_{pf}}$$

The significance of the proposed numbers (N_{HA1} and N_{HA2}) and their relations to other dimensionless groups such as Nusselt, Prandtl and Peclet numbers was thoroughly explained by Hossain and Abu-Khamsin [16, 24]. Again, substituting the above non-dimensional parameters to transform Eq. (4) into dimensionless form, and incorporating the memory concept of Eq. (1), Eq. (4) becomes:

$$k_f \frac{T_i}{L^2} \frac{\partial^2 T_f^*}{\partial x^{*2}} - \rho_f c_{pf} u_m \frac{T_i}{L} \frac{\partial T_f^*}{\partial x^*} = \phi \rho_f c_{pf} \frac{T_i k}{\phi \mu c_t L^2} \frac{\partial T_f^*}{\partial t^*} + \frac{h_c}{L} (T_f^* T_i - T_s^* T_i) \quad (15)$$

Equation (15) then reduces to:

$$\frac{k_f}{k_e} \frac{\partial^2 T_f^*}{\partial x^{*2}} - \frac{L_c \rho_f c_{pf} u_m}{k_e} \frac{L}{L_c} \frac{\partial T_f^*}{\partial x^*} = \frac{\phi \rho_f c_{pf}}{k_e} \frac{k}{\phi \mu c_t} \frac{\partial T_f^*}{\partial t^*} + \frac{h_c L_c}{k_e L_c} (T_f^* - T_s^*) \quad (16)$$

The final form of Eq. (16) thus becomes:

$$\frac{k_f}{k_e} \frac{\partial^2 T_f^*}{\partial x^{*2}} - N_{PeL} \frac{L}{L_c} \frac{\partial T_f^*}{\partial x^*} = N_{Pr} N_{HA1} \frac{\partial T_f^*}{\partial t^*} + N_{NuL} \frac{L}{L_c} (T_f^* - T_s^*) \quad (17)$$

Equations (14) and (17) are solved simultaneously for the temperature profiles (T_f^* and T_s^*) and heat transfer in terms of different rock and fluid parameters as well as different fluid velocities. The effect of memory on temperature distribution is also captured using the simultaneous solution of the model equations.

To solve the model Eqs. (14) and (17), the following dimensionless initial and boundary conditions are set by using the dimensionless parameters defined above:

$$T_f^*(x, 0) = T_s^*(x, 0) = 1, T_f^*(0, t) = T_s^*(0, t) = T_{st}/T_i, \text{ and } T_f^*(L, t) = T_s^*(L, t) = 1 \quad (18)$$

NUMERICAL SOLUTION

The conventional mass flow rate equation of the modified Darcy's law (Eq. (1)) can be used in solving these equations. However, Hossain et al. [2, 9] used a linear mass conservation based on Darcy's law. They showed that the fluid velocity was a function of the initial reservoir pressure, distance between injection and production wells, initial injection velocity, permeability of the medium, viscosity of the fluid and the pressure gradient in the formation. Hossain et al. [13, 14, 22, and 25] showed how fluid pressure and other fluid and medium properties in the formation are dependent on fluid memory. Therefore, it is important to see how memory influences the heat transfer and temperature distribution in the formation.

A finite difference method with an explicit scheme is used to solve Eqs. (14) and (17) numerically. These two equations are discretized separately due to the consideration of no thermal equilibrium between rock and fluid ($T_f^* \neq T_s^*$).

Equation (14) can be discretized as:

$$N_{Pr} N_{HA1} N_{HA2} \frac{T_{s_i}^{*n+1} - T_{s_i}^{*n}}{\Delta t^*} - \frac{k_s}{k_e} \frac{T_{s_{i+1}}^{*n} - 2T_{s_i}^{*n} + T_{s_{i-1}}^{*n}}{(\Delta x^*)^2} + N_{NuL} \frac{L}{L_c} (T_{s_i}^{*n} - T_{f_i}^{*n}) = 0 \quad (19)$$

Equation (19) can further be reduced to:

$$T_{s_i}^{*n+1} = T_{s_i}^{*n} + \frac{k_s}{k_e N_{Pr} N_{HA1} N_{HA2}} \frac{\Delta t^*}{(\Delta x^*)^2} \{T_{s_{i+1}}^{*n} - 2T_{s_i}^{*n} + T_{s_{i-1}}^{*n}\} - \frac{N_{NuL}}{N_{Pr} N_{HA1} N_{HA2} L_c} \Delta t^* (T_{s_i}^{*n} - T_{f_i}^{*n}) \quad (20)$$

The final form of Eq. (20) is thus:

$$T_{s_i}^{*n+1} = (1 - 2a_1 h - a_2 \Delta t^*) T_{s_i}^{*n} + a_1 h (T_{s_{i+1}}^{*n} + T_{s_{i-1}}^{*n}) + a_2 \Delta t^* T_{f_i}^{*n} \quad (21)$$

where, $h = \Delta t^*/(\Delta x^*)^2$, $a_1 = \frac{k_s}{k_e N_{Pr} N_{HA1} N_{HA2}}$, and $a_2 = \frac{N_{NuL}}{N_{Pr} N_{HA1} N_{HA2} L_c}$.

Similarly, Eq. (17) can be discretized as:

$$N_{Pr} N_{HA1} \frac{T_{f_i}^{*n+1} - T_{f_i}^{*n}}{\Delta t^*} + N_{PeL} \frac{L}{L_c} \frac{T_{f_{i+1}}^{*n} - T_{f_{i-1}}^{*n}}{2 \Delta x^*} - \frac{k_f}{k_e} \frac{T_{f_{i+1}}^{*n} - 2T_{f_i}^{*n} + T_{f_{i-1}}^{*n}}{(\Delta x^*)^2} + N_{NuL} \frac{L}{L_c} (T_{f_i}^{*n} - T_{s_i}^{*n}) = 0 \quad (22)$$

Equation (22) can further be reduced to:

$$T_{f_i}^{*n+1} = T_{f_i}^{*n} - \frac{\Delta t^*}{\Delta x^*} \frac{N_{PeL}}{2 N_{Pr} N_{HA1} L_c} \{T_{f_{i+1}}^{*n} - T_{f_{i-1}}^{*n}\} + \frac{\Delta t^*}{(\Delta x^*)^2} \frac{k_f}{k_e N_{Pr} N_{HA1}} \{T_{f_{i+1}}^{*n} - 2T_{f_i}^{*n} + T_{f_{i-1}}^{*n}\} - \frac{N_{NuL}}{N_{Pr} N_{HA1} L_c} \Delta t^* (T_{f_i}^{*n} - T_{s_i}^{*n})$$

(23)

The final form of Eq. (23) thus becomes:

$$T_{f_i}^{*n+1} = \{1 - 2h a_4 - a_5\} T_{f_i}^{*n} + a_5 T_{s_i}^{*n} + \{h a_4 - a_3\} T_{f_{i+1}}^{*n} + \{h a_4 + a_3\} T_{f_{i-1}}^{*n} \quad (24)$$

where, $a_3 = \frac{\Delta t^*}{\Delta x^*} \frac{N_{PeL}}{2 N_{Pr} N_{HA1}} \frac{L}{L_c}$; $a_4 = \frac{k_f}{k_e N_{Pr} N_{HA1}}$; and $a_5 = \frac{N_{NuL}}{N_{Pr} N_{HA1}} \frac{L}{L_c} \Delta t^*$.

Equations (21) and (24) are the final discretized forms of the equations for formation rock and fluid temperature distributions, respectively. Hence, dimensionless temperature profiles are obtained by solving these two equations simultaneously when the fluid and rock matrix temperatures are not equal.

RESULTS AND DISCUSSION

Computations are carried out for a reservoir 3,000 meters long where steam is injected at a constant rate of 17.5 m^3 of equivalent water volume per day. All assumed rock and fluid parameters are listed in Table 1. The time and distance steps are set at $\Delta x^* = 0.0167$ and $\Delta t^* = 0.00001$. Temperature variation is obtained for the case where the fluid and rock temperatures are considered not equal (i.e. $T_s \neq T_f$).

In Eq. (17), the local Peclet number can be defined as $(N_{Pe})_L = L_c \rho_f c_{pf} u_m / k_e$ where L_c represents a characteristic length such as the mean pore throat diameter of the porous medium. During the computation, L_c is calculated by Kolodzie's correlation [26]: $L_c = 2\pi r_{pt}$ where $\log r_{pt} = 0.732 + 0.588 \log k - 0.864 \log \phi$. In this correlation, k is in mD and r_{pt} is in microns. Kolodzie [26] and Pittman [27] proposed this correlation as the best permeability estimator for sandstones. They and others [28] indicated that the best results are obtained from a mercury injection capillary pressure test at 35% mercury saturation. Other correlations for carbonate rocks are also proposed in the same literature.

Since the Nusselt number, N_{Nu} , refers to the ratio of total to conductive heat transfer, the local Nusselt number with respect to wellbore position and reservoir boundary can be defined as $(N_{Nu})_{x^*} = [\partial T^* / \partial y^*]_{x^*=0,1}$. It can also be calculated using $(N_{Nu})_{x^*} = h_c x^* / k_e$.

Figures 2(a – b) show the variations of dimensionless temperature (T^*) with dimensionless distance (x^*) or time (t^*) for two fluid velocities: $u_m = 0.000001 \text{ m/s}$ and 0.001 m/s . The temperature profile with distance shows that the rock temperature profile and the fluid temperature profile do not change with fluid velocity for a given time (e.g., $t^* = 0.33333$ or 0.66667) and the rock gains more heat compared with the fluid at the same time (Figure 2(a)). The temperature profiles move forward with time but at higher temperatures. Again, the temperature profile with time shows that the rock temperature profile and the fluid temperature profile do not change with fluid velocity for a given distance (e.g., $x^* = 0.32258$ or 0.64516) and the rock gains more heat compared with the fluid at the same distance (Figure 2(b)). Around the injection well, heat transfer and temperature propagation are more pronounced with time. On the other hand, towards the outer boundary (the production well), there is no change in the temperature profile (Figure 2(b)).

Figures 3(a – b) show variations of dimensionless temperature (T^*) with N_{HA1} for different combinations of fluid velocity (u_m) and dimensionless distance (x^*) for a fixed $t^* = 0.66301$ (Fig. 2(a)) or combinations of fluid velocity (u_m) and dimensionless time (t^*) for a fixed $x^* = 0.16129$ (Fig. 3(b)). The temperature profile decreases nonlinearly with N_{HA1} for different u_m and x^* (Figure 3(a)). Temperature profile is more pronounced closer to the injection well with higher rock temperature distribution (Figure 3(a)). Here, the temperature profile is strongly effected by N_{HA1} especially around the injection well. The temperature profile again decreases nonlinearly with N_{HA1} for different u_m and t^* (Figure 3(b)). Temperature profile is more pronounced with time and rock temperature distribution is higher than that of fluid temperature. Here temperature profile is strongly effected by N_{HA1} , u_m , and t^* .

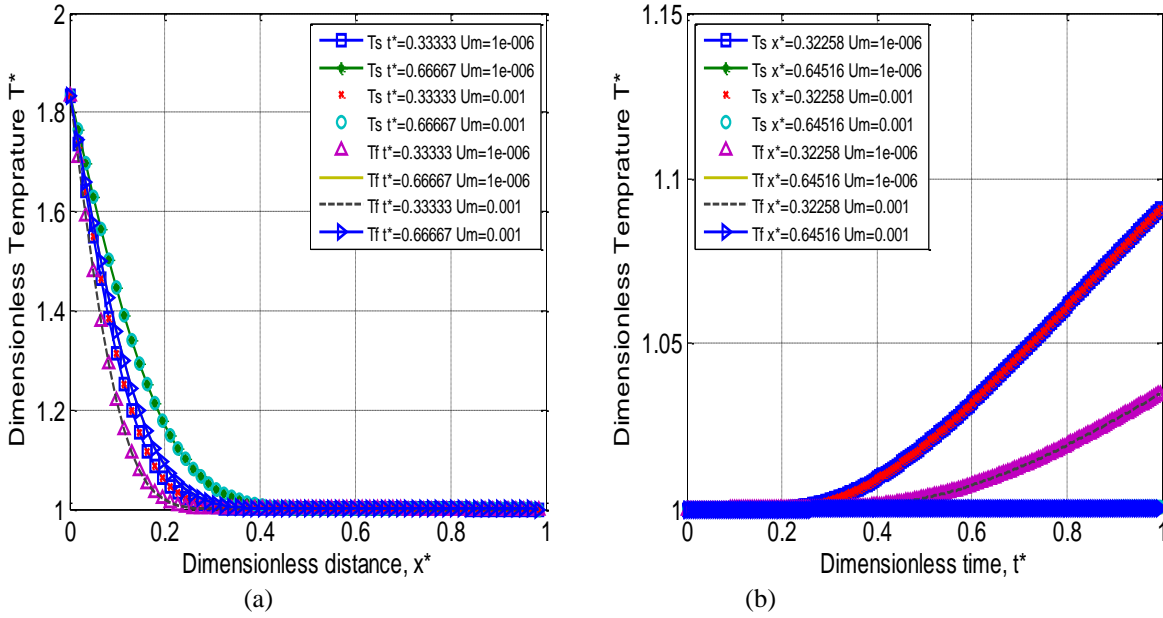


Figure 2. Variation of dimensionless temperature (T^*) with dimensionless distance (x^*) or time (t^*) for for two fluid velocities (u_m).

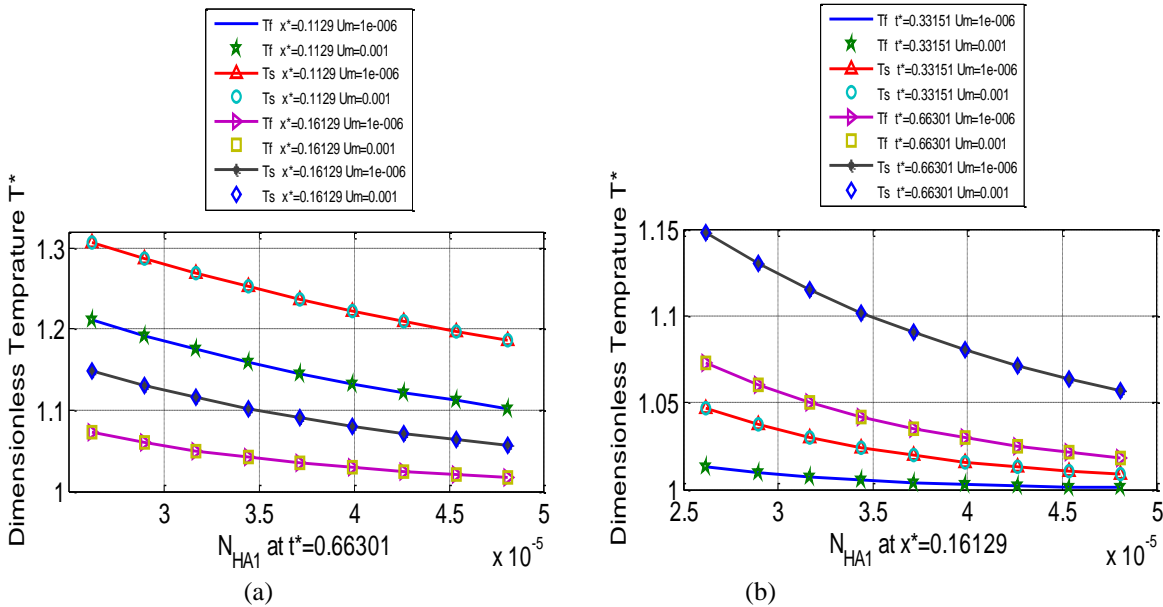
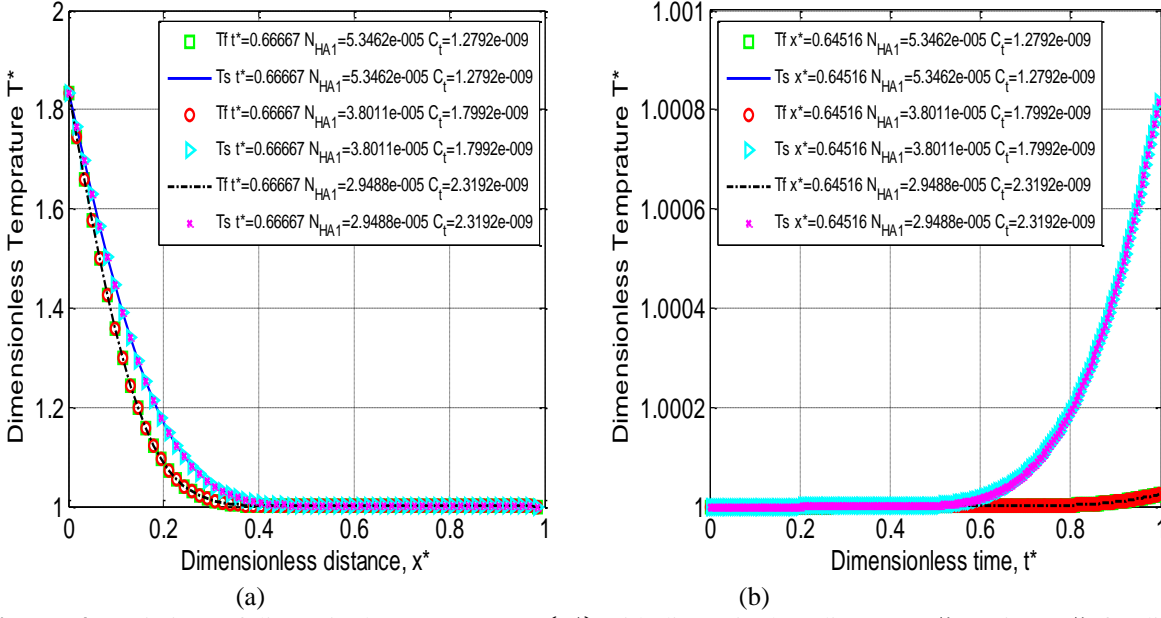


Figure 3. Variation of dimensionless temperature (T^*) with N_{HA1} at a fixed dimensionless time (e.g. $t^* = 0.66301$) or at a fixed dimensionless distance (e.g. $x^* = 0.16129$) for two fluid velocities (u_m).

Figures 4(a – b) depict variations of dimensionless temperature (T^*) with dimensionless distance (x^*) or time (t^*) for different sets of N_{HA1} and c_t values. Figure 3(a) is at $t^* = 0.66667$ while Figure 4(b) is at $x^* = 0.64516$. The temperature profile decreases with distance and becomes stabilized at a distance of approximately $x^* = 0.42$ for rock and $x^* = 0.38$ for fluid where there is no traceable effects of N_{HA1} and c_t on either the rock or fluid temperature profiles (Figure 4(a)). Here, the rock shows temperatures that are higher than those of the fluid. Figure 4(b) shows the rock and fluid to begin gaining temperature at approximately $t^* = 0.57$ and $t^* = 0.64$, respectively. However, the rock matrix heats up faster than the interstitial fluid as a result of hot fluid injection for the same $x^* = 0.64516$, and there is no traceable effects of N_{HA1} and c_t on the temperature profile.



Figures 4. Variations of dimensionless temperature (T^*) with dimensionless distance (x^*) or time (t^*) for different N_{HA1} and c_t values.

Figures 5(a – b) depict the variation of dimensionless temperature (T^*) with dimensionless distance (x^*) or time (t^*) for different sets of N_{HA1} and fluid viscosity (μ) values. Figure 5(a) is at $t^* = 0.66667$ while Fig. 4(b) is at $x^* = 0.64516$. The temperature profile decreases with distance and become stabilized at a distance of approximately $x^* = 0.43$ for rock and $x^* = 0.39$ for fluid and there are no traceable effects of N_{HA1} and μ on both rock and fluid temperature profiles (Figure 5(a)). Here, the rock temperature profile is higher than that of the fluid. Figure 5(b) shows the rock and fluid begin to gain temperature at approximately $t^* = 0.52$ and $t^* = 0.62$, respectively. The rock gains heat faster than the interstitial fluid at the same $x^* = 0.64516$ and there are no traceable effects of N_{HA1} and μ on the temperature profile. The patterns of the two temperature distributions are similar to those observed in Figures 4(a – b).

Figures 6(a – b) depict the variation of dimensionless temperature (T^*) with dimensionless distance (x^*) or time (t^*) for different values of (N_{HA1}) and fluid density (ρ_f). Figure 6(a) is at $t^* = 0.66667$ while Fig. 6(b) is at $x^* = 0.64516$. The temperature decreases with distance and becomes stabilized at different distances of approximately $x^* = 0.58, 0.5$ and 0.4 , respectively, with the increase of ρ_f and N_{HA1} for the rock (Figure 5(a)). The same trend is seen in the fluid temperature at different stabilization distances: $x^* = 0.4, 0.36$, and 0.3 . This figure confirms that there is an effect of N_{HA1} and ρ_f on the temperature distribution of rock and fluid (Figure 6(a)). The temperature starts to increase with time at approximately $t^* = 0.41, 0.6$ and 0.78 , respectively with increase in ρ_f and N_{HA1} for the rock (Figure 6(b)). The same trend is seen in the fluid temperature at different stabilization times: $t^* = 0.56, 0.78$, and 0.9 . With increase in N_{HA1} and ρ_f , the temperature starts to decrease which confirms the effect of N_{HA1} and ρ_f on the temperature distributions of both rock and fluid (Figure 6(b)).

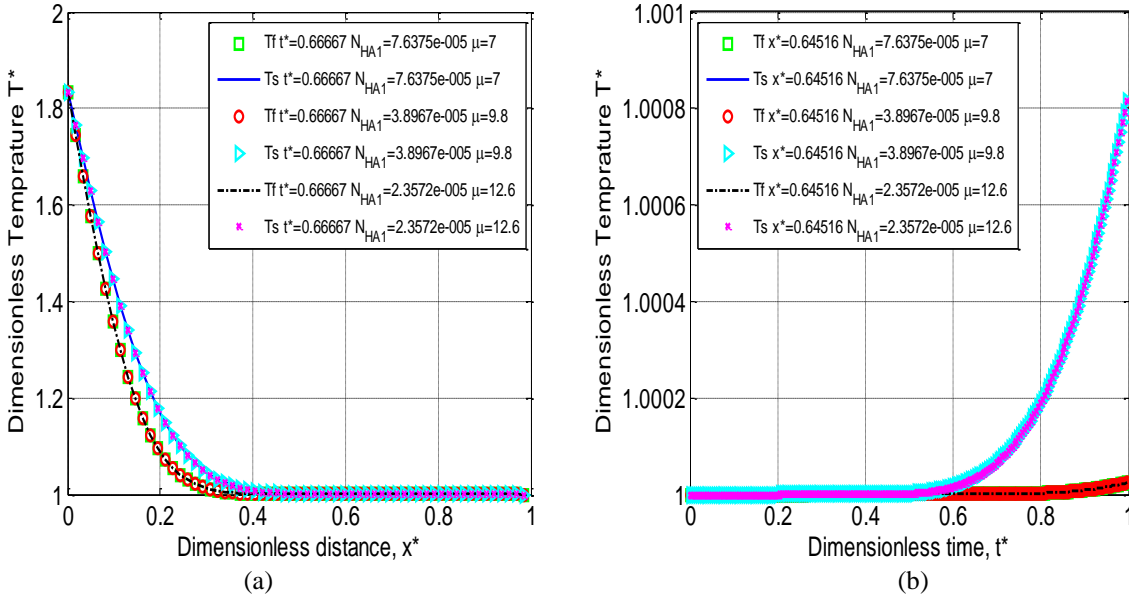


Figure 5. Variation of dimensionless temperature (T^*) with dimensionless distance (x^*) or time (t^*) for various N_{HA1} and μ values.

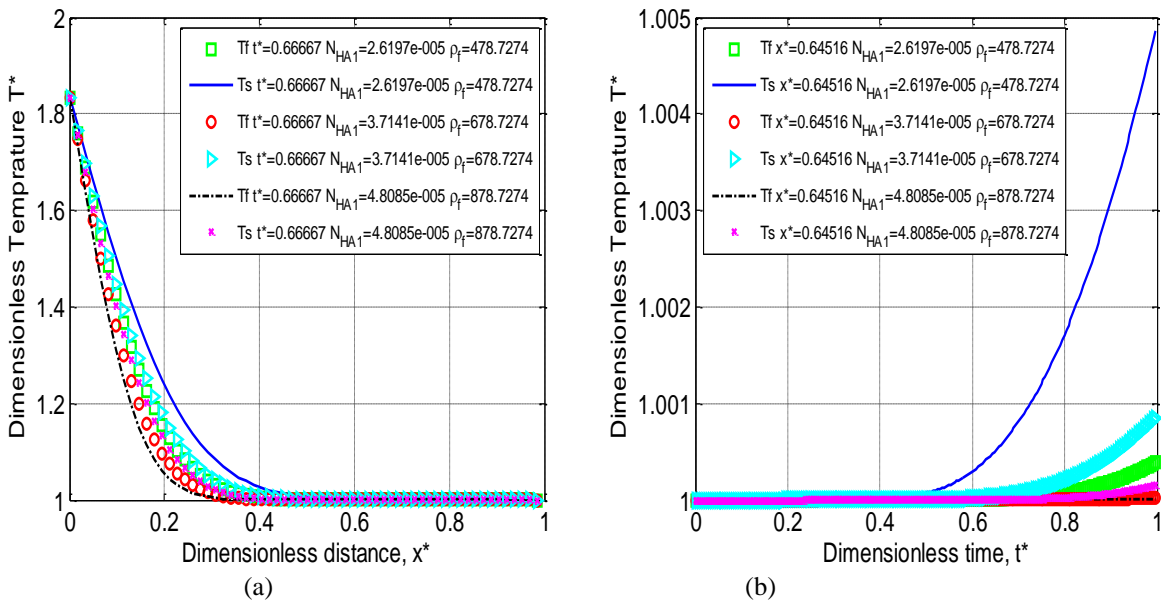


Figure 6. Variation of dimensionless temperature (T^*) with dimensionless distance (x^*) or time (t^*) for different N_{HA1} and ρ_f values.

Figures 7(a – b) depict the variation of dimensionless temperature (T^*) with dimensionless distance (x^*) or time (t^*) for different sets of (N_{HA1}) and permeability (k) values. Figure 7(a) is at $t^* = 0.66667$ while Fig. 7(b) is at $x^* = 0.64516$. The temperature decreases with distance and become stabilized at different distances of approximately $x^* = 0.42, 0.2$ and 0.15 respectively with the increase of k and N_{HA1} for rock (Figure 6(a)). The same scenario is seen for fluid temperature at a different stabilization distance, $x^* = 0.38, 0.16$, and 0.12 respectively. This figure conform that there is an effect of N_{HA1} and k on the temperature distribution of rock and fluid (Figure 7(a)). The temperature of rock starts to increase with time at approximately $t^* = 0.56$ for $k = 10^{-14}m^2$ and $N_{HA1} = 3.7424$. As permeability and N_{HA1} increase, there is no change of temperature of rock (Figure 7(b)). The same scenario is seen for fluid temperature at a different stabilization time, $t^* = 0.62$. Therefore, it can be concluded that with the increase of N_{HA1} and k , temperature starts to decrease which conforms that there is a strong effect of N_{HA1} and k on the temperature distribution of rock and fluid (Figure 7(b)).

Figures 8(a) and 8(b) depict the variation of dimensionless temperature (T^*) with (N_{HA2}) for different porosity, (ϕ), and $\rho_f c_{pf}$ values at $t^* = 0.663013$ and $x^* = 0.1290$, respectively. There is no change in dimensionless fluid temperature with N_{HA2} when porosity changes (Figure 8(a)), within the range studied in this work. However, solid rock dimensionless temperature increases with the increase of porosity. An increase in porosity increases convection, but decreases the relative

volume of the solid phase. Any reduction in solid volume (and mass) will increase the rate of heating for a given amount of heat injected into the system. While increased convection will reduce the solid temperature, increased rate of heating will increase solid temperature. These counteracting phenomena give rise to the existence of an optimal value, for which solid temperature will begin to decrease. However, this optimal value has not been investigated in this paper. The same trend is depicted in Figure 8(b).

Figure 8 also indicates that the solid temperature is consistently higher than fluid temperature. This behavior is not unexpected. In a porous medium, both solid mass and conductivity (see Table 1) are much higher than liquid mass and conductivity, respectively. This results in faster heat transfer within the solid phase. Heat transfer within the fluid phase is mainly through convection, which depends largely on the flow rate. Higher injection rate will increase the convection, resulting in faster dissipation of heat within the fluid phase. However, the solid phase will remain relatively less affected because the role of convection is limited to rock-fluid interaction within the solid phase. It is possible that within certain injection rates, the temperature trends will reverse, but it was not investigated in this work.

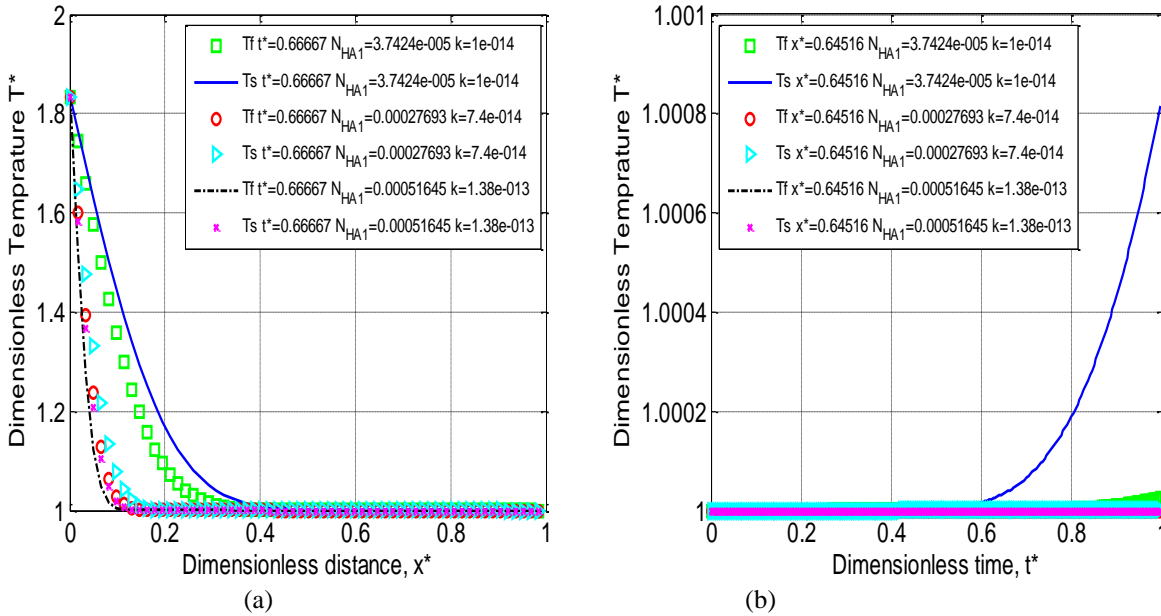


Figure 7. Variation of dimensionless temperature (T^*) with dimensionless distance (x^*) or time (t^*) for different N_{HA1} and k values.

Figures 9(a – f) depict the variation of dimensionless temperature (T^*) with permeability, k , at $t^* = 0.663013$ for three different dimensionless distances, $x^* = 0.1129, 0.16129$ and 0.32258 . Permeability of the porous medium increases with the increase of fluid temperature for all the three cases at the same time (Figures 9(a, c, and e)). Permeability increases more around the wellbore and closer to the injection well. However, permeability increase continues with slight increase of temperature at the outer boundary of the reservoir or toward the production well. This indicates that temperature profile influences the permeability value and the higher the temperature the greater the permeability throughout the reservoir. Again, as solid temperature decreases, permeability increases and more responsive around the injection well (Figures 9(b, d, and f)). The temperature profile is nonlinear in nature for both solid and rock temperature profiles.

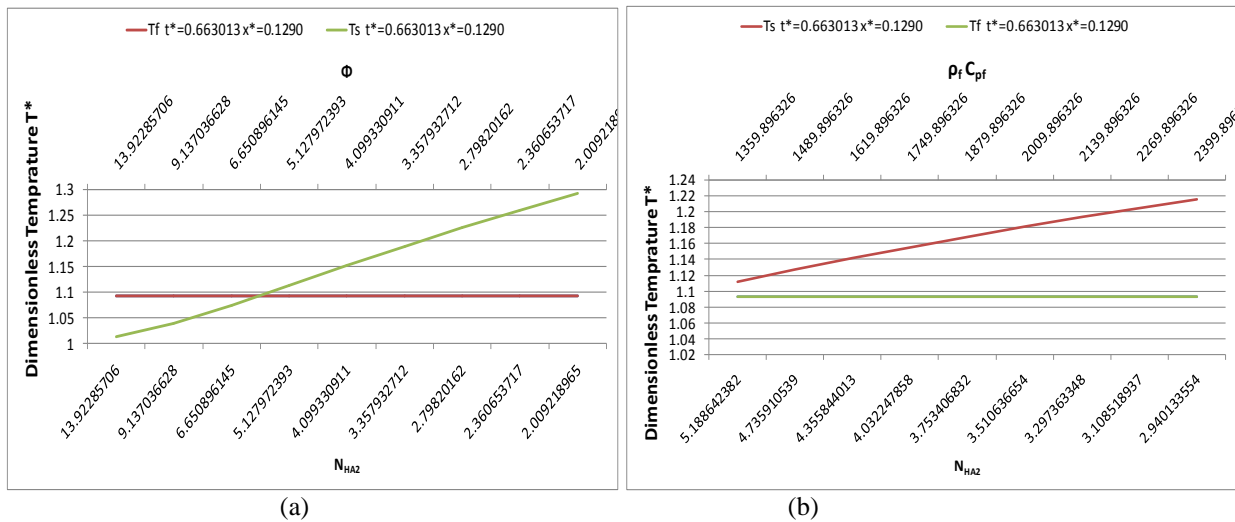


Figure 8. Variation of dimensionless temperature (T^*) with (N_{HA2}) for different porosity and $\rho_f c_{pf}$ values.

Figures 10(a–b) depict the variation of dimensionless temperature (T^*) with dimensionless distance (x^*) at $t^* = 0.66667$ but for different sets of N_{NuL} and k_e or L_c values. The temperature profile decreases with distance and become stabilized at a distance of approximately $x^* = 0.40$ for rock and $x^* = 0.30$ for fluid where there is no traceable effects of N_{NuL} , k_e , and L_c pronounced for both rock and fluid temperature profile individually. Moreover, solid temperature profile is always higher than that of fluid temperature profile. Figures 10(c–d) depict the variation of dimensionless temperature (T^*) with dimensionless time (t^*) at a given distance ($x^* = 0.64516$) for the same set of variables as in Figs. 10(a–b). Here, rock temperature distribution is higher than that of fluid temperature as stated earlier. The rock and fluid start to gain temperature at approximately $t^* = 0.58$ and $t^* = 0.7$ respectively. The trend and behavior of the figures are same as stated for Figure 5(b) and 6(b). It is clear that there is no traceable effects of N_{NuL} , k_e , and L_c on the temperature profile.

Figures 11(a–d) depict the variation of dimensionless temperature (T^*) with dimensionless distance (x^*) at $t^* = 0.66667$ for different Peclet numbers (N_{PeL}) with different (L_c), (k_e), u_m , and ($\rho_f c_{pf}$) values, respectively. The trend and behavior are the same as seen in Figures 10(a–b). There is no change of temperature profile for L_c , k_e , and u_m which indicate that those parameters do not have any significant influence on temperature profile. However, temperature distribution has an increasing trend for increase in $\rho_f c_{pf}$. Rock and fluid temperature profiles show significant differences.

Figures 12(a – d) depict the variation of dimensionless temperature (T^*) with dimensionless time (t^*) for different Peclet numbers (N_{PeL}), and different (L_c), (k_e), u_m , and ($\rho_f c_{pf}$) values, respectively at $x^* = 0.64516$. The trend and behavior are the same as seen in Figures 10(c – d). There is no significant change of temperature profile for L_c , k_e , and u_m which indicates that those parameters do not have any significant influence on temperature profile. However, temperature distribution has an increasing trend for the increase of $\rho_f c_{pf}$ (Figure 12(d)).

Figures 13(a–c) depict the variation of dimensionless temperature (T^*) with dimensionless distance (x^*) for different Prandtl numbers (N_{Pr}) and different (k_e), c_{pf} , and (μ) values, respectively at $t^* = 0.66667$. There are no significant effects of N_{Pr} , k_e , and μ on dimensionless fluid and solid temperature distributions (Figures 13 (a, c)). The trend and behavior are the same as seen in Figures 11(a – c). Both dimensionless solid and fluid temperatures decrease with distance when N_{Pr} and c_{pf} increases (Figures 13 (b)). This indicates that both N_{Pr} and c_{pf} have significant effects on temperature distribution which is similar to Figure 11(d). For all the figures, both rock and fluid temperatures have significant differences.

Figures 14(a – c) depict the variation of dimensionless temperature (T^*) with dimensionless time (t^*) for different Prandtl numbers (N_{Pr}), and different (k_e), c_{pf} , and (μ) values, respectively at $x^* = 0.64516$. The three figures show that rock temperature is more sensitive to N_{Pr} , k_e , and μ compared with fluid temperature. Fluid dimensionless temperature is less sensitive at the initial stage of steam flooding (Figures 14(a,c)). However, the temperature profile is more pronounced when N_{Pr} , c_{pf} changes with time (Figures 14(b)). This is true for both solid and rock temperatures where rock temperature is very sensitive.

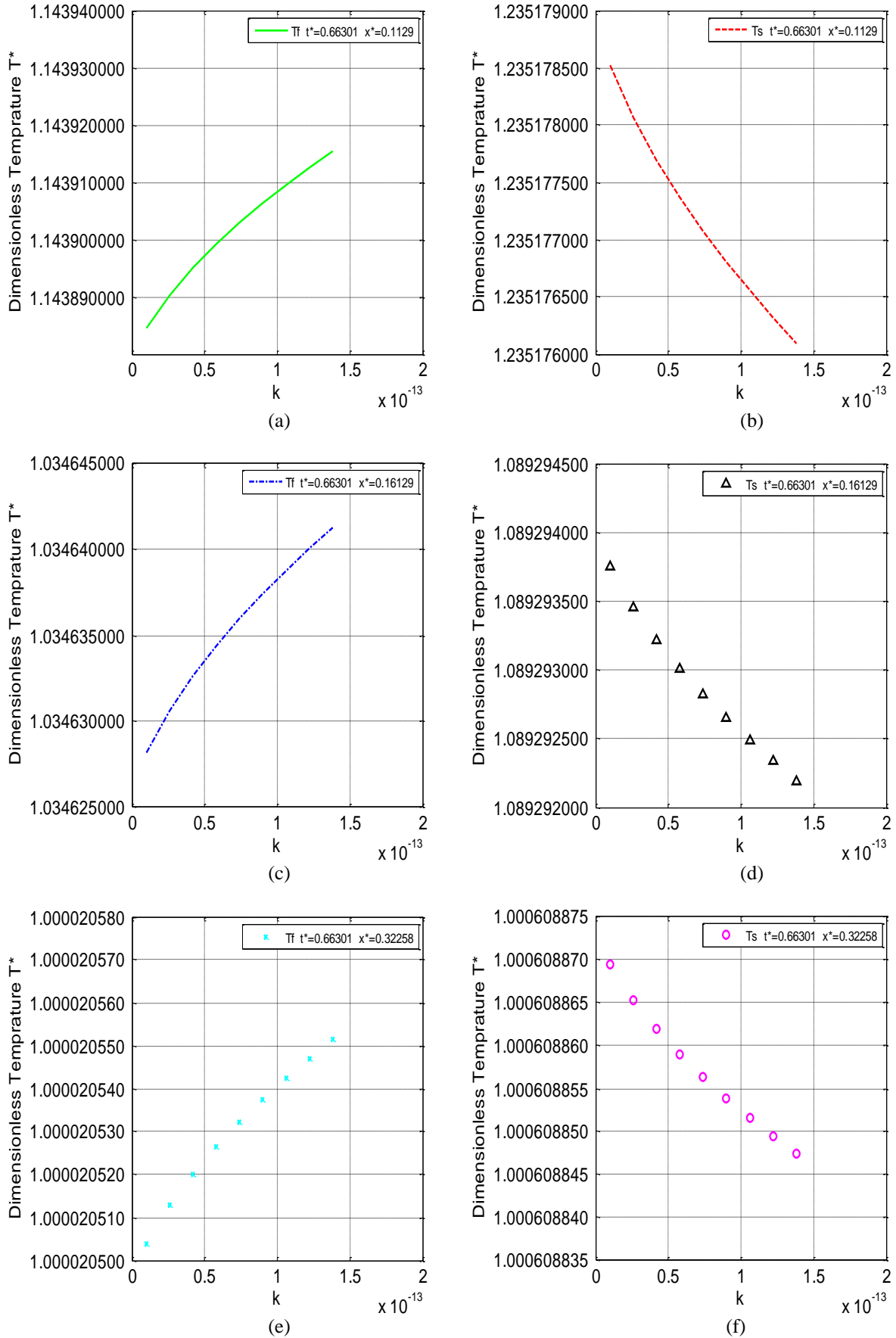


Figure 9. Variation of dimensionless temperature (T^*) with permeability (k) for a given time (t^*) at three locations (x^*).

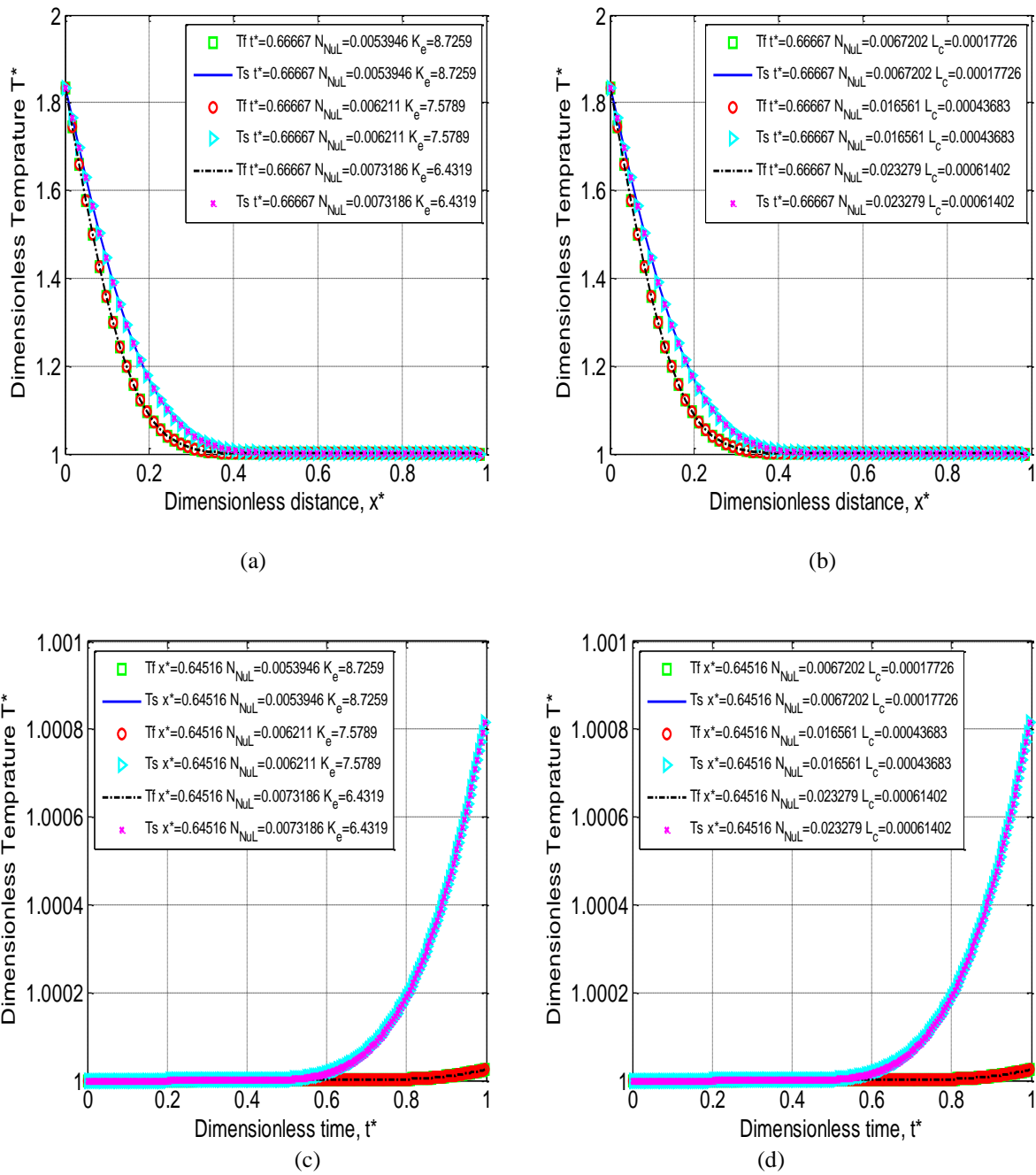


Figure 10. Variation of dimensionless temperature (T^*) with dimensionless distance (x^*) or time (t^*) for different Nusselt number (N_{NUL}), (k_e) and (L_c) values.

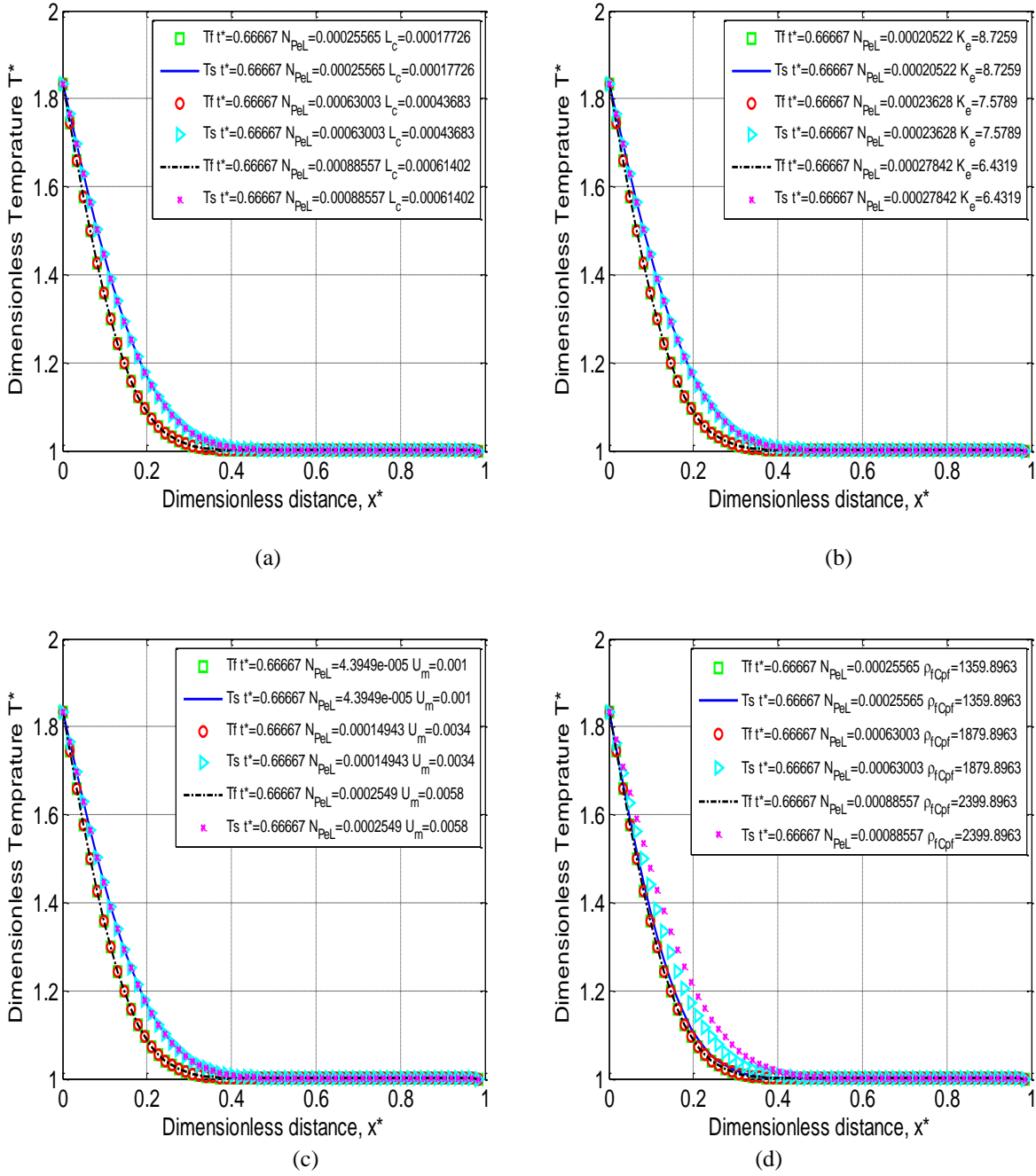


Figure 11. Variation of dimensionless temperature (T^*) with dimensionless distance (x^*) for different Peclet numbers (N_{PeL}), and different (L_c), (k_e), u_m , and ($\rho_f c_{pf}$) values.

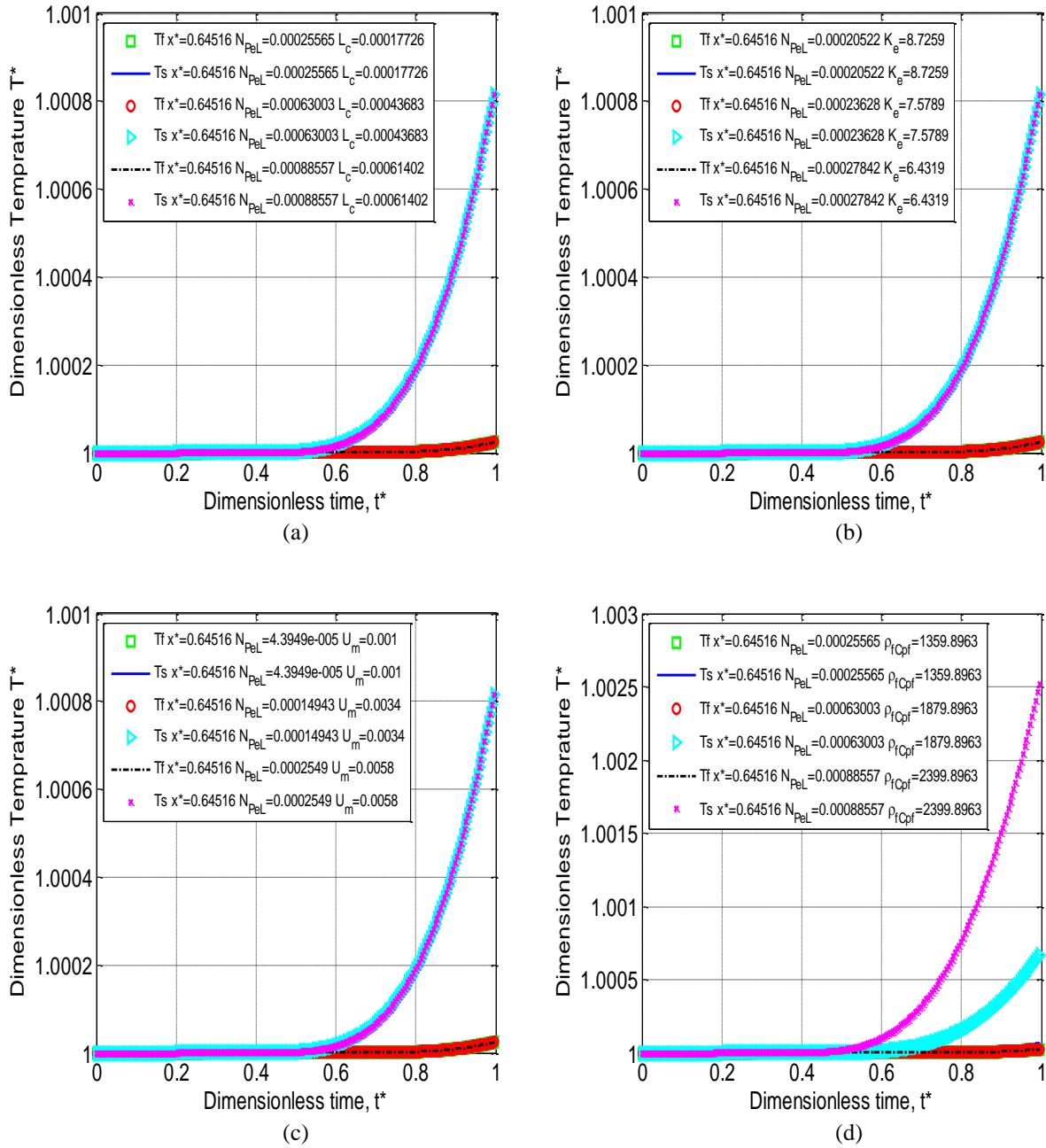


Figure 12. Variation of dimensionless temperature (T^*) with dimensionless time (t^*) for different Peclet numbers (N_{PeL}), and different (L_c), (k_e), u_m and ($\rho_f C_{pf}$) values at a given distance.

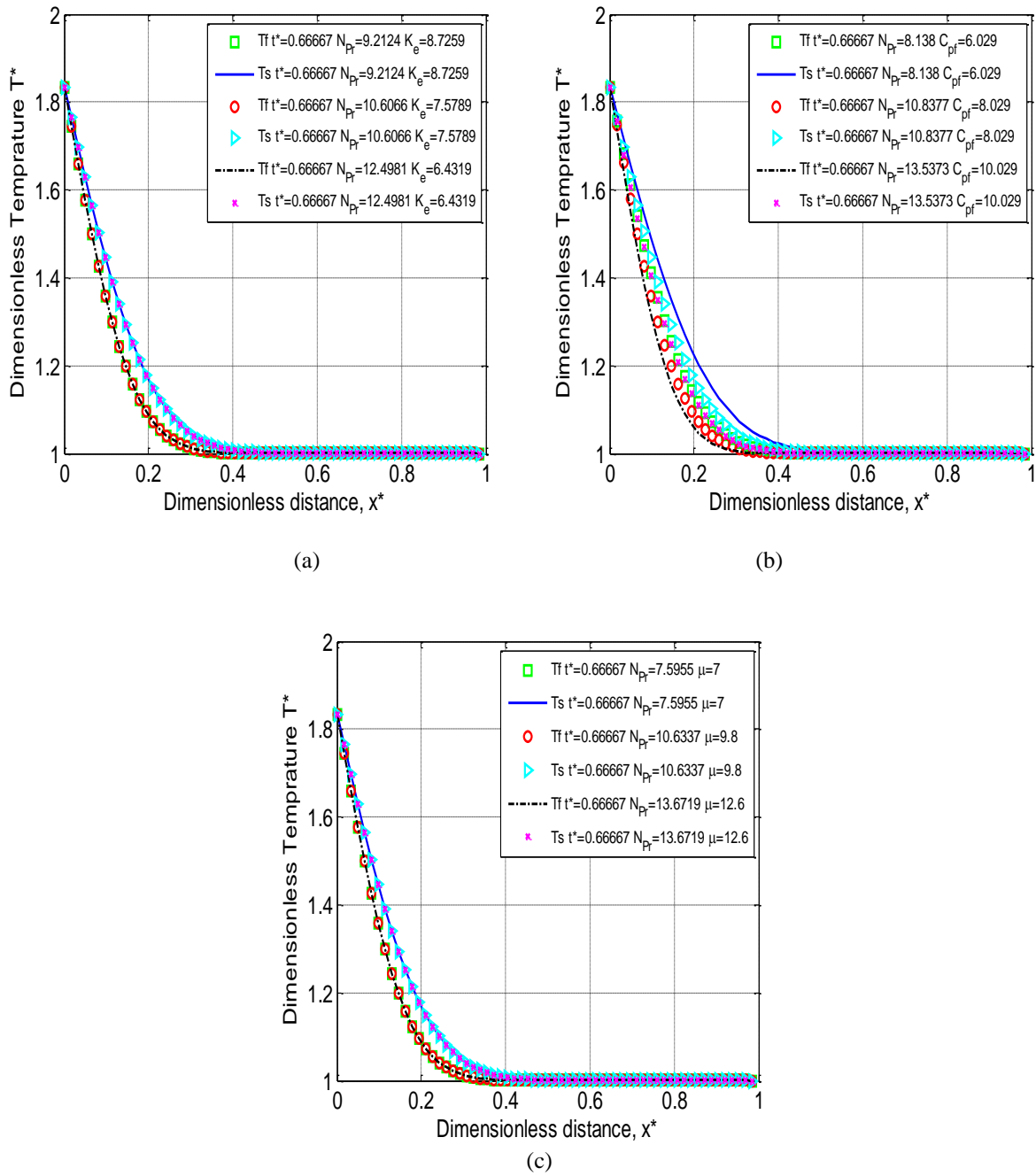


Figure 13. Variation of dimensionless temperature (T^*) with dimensionless distance (x^*) for different Prandtl numbers (N_{Pr}), and different (k_e), (C_{pf}), and (μ) values at a fixed t^* .

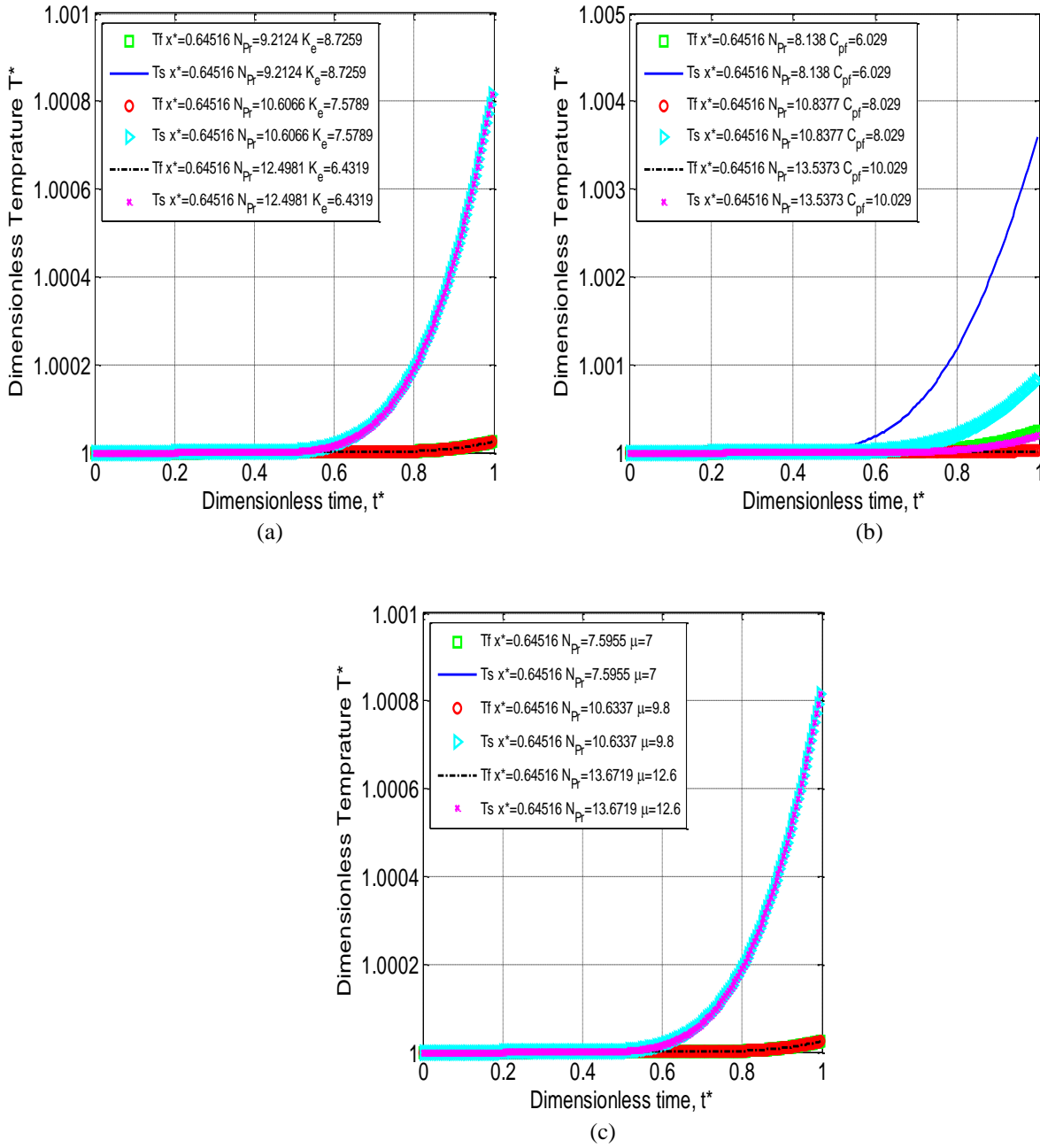


Figure 14. Variation of dimensionless temperature (T^*) with dimensionless time (t^*) for different Prandtl numbers (N_{Pr}), and different (k_e), (c_{pf}), and (μ) values at a fixed x^* .

CONCLUSIONS

A set of mathematical models with the inclusion of “memory” concept is developed to investigate the temperature propagation for a thermal flooding operation. The proposed models are well capable of handling the variable rock and fluid properties with time and space. Two dimensionless numbers are also proposed that are able to explain the rheological behavior of the system when continuous alteration phenomena happen within the porous medium. Results show that both rock and fluid temperature profiles are sensitive to space, time, system rheological properties, and fluid velocity. The effects of temperature on different reservoir parameters can be investigated using the proposed mathematical tool and dimensionless numbers.

NOMENCLATURE

Latin Symbols

- c_f = total fluid compressibility of the system, $1/pa$
 c_s = formation rock compressibility of the system, $1/pa$
 c_t = total compressibility of the system, $1/pa$
 c_{pf} = specific heat capacity of injected fluid, kJ/kgK
 c_{pg} = specific heat capacity of steam, kJ/kgK
 c_{po} = specific heat capacity of oil, kJ/kgK
 c_{ps} = specific heat capacity of solid rock matrix, kJ/kgK
 c_{pw} = specific heat capacity of water, kJ/kgK
 h_c = convection heat transfer coefficient, kJ/hm^2K
 k = original porous medium permeability, m^2
 k_e = effective thermal conductivity of the system, $kJ/h m K$
 k_f = thermal conductivity of fluid, $kJ/h m K$
 k_g = thermal conductivity of gas, $kJ/h m K$
 k_o = thermal conductivity of oil, $kJ/h m K$
 k_s = thermal conductivity of solid rock matrix, $kJ/h m K$
 k_w = thermal conductivity of water, $kJ/h m K$
 L = distance between production and injection well along x direction, m
 $L_c = 2\pi r_{pt}$ = characteristic length i.e. pore throat diameter of the porous media, m
 L^* = dimensionless length of the reservoir
 M = average system heat capacity, kJ/m^3K
 $N_{NuL} = h_c L_c / k_e$ = local Nusselt number, dimensionless
 $N_{PeL} = L_c \rho_f c_{pf} u_m / k_e$ = local Peclet number, dimensionless
 $N_{Pr} = \mu c_{pf} / k_e$ = pseudo Prandtl number, dimensionless
 p = pressure of the system, pa
 p_i = initial pressure of the system, pa
 $q_i = Au$ = initial volume production rate, m^3/s
 $q_{prod} = Au$ = production volume flow rate of oil, m^3/s
 r_{pt} = pore-throat radius, microns
 S_g = gas saturation, volume fraction
 S_o = oil saturation, volume fraction
 S_w = water saturation, volume fraction
 t = time, s
 T = temperature, K
 T^* = dimensionless temperature
 T_f = fluid temperature, K
 T_i = initial reservoir temperature, K
 T_r = reference temperature of injected fluid, K
 T_s = average temperature of solid rock matrix, K
 T_{st} = temperature of injected steam, K
 t^* = dimensionless time
 u_m = fluid velocity in terms of memory, m/s
 u^* = dimensionless velocity
 x = flow dimension at any point along x-direction, m
 x^* = dimensionless distance

Greek Symbols

- α = fractional order of differentiation, dimensionless
 $\nu = \mu / \rho_f$ = kinematic viscosity (ratio of absolute or dynamic viscosity to density), m^2/s
 η = ratio of the pseudopermeability of the medium with memory to fluid viscosity, $m^3 s^{1+\alpha} / kg$
 μ = fluid dynamic viscosity, $pa s$
 μ_i = initial fluid dynamic viscosity, $pa s$

- ξ = a dummy variable for time i.e. real part in the plane of the integral, s
 Γ = gamma function
 ρ = fluid density, kg/m^3
 ϕ = porosity of the rock, volume fraction
 ϕ_i = initial porosity of the rock, volume fraction
 ρ_f = density of fluid, kg/m^3
 ρ_g = density of gas, kg/m^3
 ρ_o = density of oil, kg/m^3
 ρ_s = density of solid rock matrix, kg/m^3
 ρ_w = density of water, kg/m^3

ACKNOWLEDGEMENTS

The authors would like to thank King Fahd University of Petroleum & Minerals (KFUPM) for funding this work under project number JF100009. The authors are also grateful for the support and guidance received from KFUPM's Deanship of Scientific Research.

REFERENCES

- [1] Siemek, J and Stopa, J. (2002). A Simplified Semi-Analytical Model for Water-Coning Control in Oil Wells with Dual Completions System. *Journal of Energy Resources Technology; Transactions of the ASME*, vol. 124, no., 4, pp. 246-252.
- [2] Hossain, M.E., Mousavizadegan, S.H. and Islam, M.R. (2008). The Effects of Thermal Alterations on Formation Permeability and Porosity. *Petroleum Science and Technology*, 26(10-11), pp. 1282 – 1302.
- [3] Hossain, M.E., Mousavizadegan, SH and Islam, M.R. (2009). Rock and fluid temperature changes during thermal operations in EOR processes. *Journal Nature Science and Sustainable Technology*, 2(3), 347 – 378.
- [4] Kaye, S.E., Ting, V.C., and Fair, I.C. (1982). Development of a System to Utilize Flue Gas from Enhanced Oil Recovery Combustion Projects. *Journal of Petroleum Technology*. January, 181 – 88.
- [5] Chu, C. (1983). Current In-Situ Combustion Technology. *Journal of Petroleum Technology*. August, 1412 – 1420.
- [6] Khan, M.M., Prior, D., and Islam, M.R. (2005). Direct-Usage solar Refrigeration: From Irreversible Thermodynamics to Sustainable Engineering. presented in Jordan International Chemical Engineering Conference, V. 12-14 September, Amman, Jordan paper no - JICEC05-CHE-4-27.
- [7] Yoshioka, K, Zhu, D, Hill, AD, Dawkrajai, P and Lake, LW. (2006). Detection of Water or Gas Entries in Horizontal Wells from Temperature Profiles. SPE – 100209, presented at SPE Europepec/EAGE annual conference and exhibition, Vienna, Austria, June 12-15, 2006.
- [8] Dawkrajai, P, Lake, LW, Yoshioka, K, Zhu, D and Hill, AD (2006). Detection of water or gas entries in horizontal wells from temperature profiles. SPE – 100050, presented at SPE/DOE symposium on improved oil Recovery, Tulsa, Oklahoma, USA, April 22-26.
- [9] Hossain, M.E., Mousavizadegan, S.H. and Islam, M.R. (2009a). Variation of Rock and Fluid Temperature during Thermal Operations in Porous Media. *Petroleum Science and Technology*, 27, pp. 597 – 611
- [10] Hossain, ME. An Experimental and Numerical Investigation of Memory-Based Complex Rheology and Rock/Fluid Interactions. PhD dissertation, Dalhousie University, Halifax, Nova Scotia, Canada. 2008; 773.
- [11] Yoshioka, K, Zhu, D, Hill, AD and Lake, LW. (2005). Interpretation of temperature and pressure profiles measured in multilateral wells equipped with intelligent completions. SPE – 94097, presented at SPE Europepec/EAGE annual conference, Madrid, Spain, June 13 – 16, 2005.
- [12] Yoshioka, K, Zhu, D, Hill, AD, Dawkrajai, P and Lake, LW. (2005). A Comprehensive Model of Temperature Behavior in a Horizontal Well. SPE – 95656, presented at SPE Annual Technical Conference and Exhibition, Dallas, Texas, USA, October 09 – 12.
- [13] Hossain, M.E., Mousavizadegan, SH, Ketata, C and Islam, MR. A novel memory based stress-strain model for reservoir characterization. *Journal Nature Science and Sustainable Technology*, 2007; 1(4): 653 – 678.
- [14] Hossain, M.E., Mousavizadegan, S.H. and Islam, M.R. (2009b). Effects of Memory on the Complex Rock-Fluid Properties of a Reservoir Stress-Strain Model. *Petroleum Science and Technology*, 27 (10), pp. 1109 – 1123.
- [15] Spillette, A.G. Heat transfer during hot fluid injection into an oil reservoir. *J Cdn. Pet. Tech.*, 1965; Oct. – Dec.: 34 – 39.
- [16] Hossain, M.E. and Abu-Khamsin, S.A. (2012). Development of Dimensionless Numbers for Heat Transfer in Porous Media Using Memory Concept. *Journal of Porous Media*, accepted for publication, Track Number: 10-STRPM-182-10-JPM-2024 and BH ID: JPM-2799, vol 15, in press.
- [17] Chan, Y.T., and Banerjee, S. (1981). Analysis of Transient Three-Dimensional Natural Convection in Porous Media. *J. Heat Transfer* 103:242–248.
- [18] Kaviany, M. (2002). Principles of heat transfer. New York: John Wiley & Sons, pp. 885–897.

-
- [19] Hossain, M.E. and Islam, M.R. (2009). An Advanced Analysis Technique for Sustainable Petroleum Operations. VDM Verlag Dr. Muller Aktiengesellschaft & Co. KG, Germany, pp. 655.
- [20] Caputo, M. (1999). Diffusion of Fluids in Porous Media with Memory. *Geothermics*, Vol. 23, pp. 113 – 130.
- [21] Caputo, M., (2000). Models of Flux in Porous Media with Memory. *Water Resources Research*, Vol. 36(3), pp. 693 – 705.
- [22] Hossain, M.E., Mousavizadegan, S.H. and Islam, M.R. (2008). A New Porous Media Diffusivity Equation with the Inclusion of Rock and Fluid Memories. *SPE– 114287-MS, E-Library, Society of Petroleum Engineers*.
- [23] Marx, J.W. and Langenheim, R.H. (1959). Reservoir Heating by Hot Fluid Injection, *Trans. AIME*, 216.
- [24] Hossain, M.E. and Abu-Khamsin, S.A. (2010b). Utilization of Memory Concept to Develop Heat Transfer Dimensionless Numbers for Porous Media Undergoing Thermal Flooding with Equal Rock-Fluid Temperatures. submitted to *Journal of Porous Media*, Track Number: 10-JPM-2048 and BH ID: 10-JPM-2903, under review
- [25] Hossain, M.E., Liu, L. and Islam, M. R. (2009). Inclusion of the Memory Function in Describing the Flow of Shear-Thinning Fluids in Porous Media. *International Journal of Engineering (IJE)*, 3(5), pp. 458 – 477.
- [26] Kolodzie, S. Jr. (1980). Analysis of pore throat size and use of the Waxman-Smits equation to determine OOIP in Spindle Field, Colorado Society of Petroleum Engineers, 55th Annual Fall Technical Conference Paper 9382, 10p
- [27] Pittman, E.D. (1992). Relationship of Porosity and Permeability to various Parameters Derived from Mercury Injection-Capillary Pressure Curve for Sandstone AAPG Bulletin, 76, pp. 191–198.
- [28] Rezaee, M.R., Jafari, A. and Kazemzadeh, E. (2006). Relationships between permeability, porosity and pore throat size in carbonate rocks using regression analysis and neural networks. *J. Geophys. Eng.*, 3, pp. 370–376.

Table 1: Fluid and rock properties for numerical computations

Fluid or rock property	Fluid or rock property
$c_{pg} = 29.7263 [kJ/kg - K]$	$S_g = 20\% [vol/vol]$
$c_{po} = 2.0934 [kJ/kg - K]$	$S_o = 60\% [vol/vol]$
$c_{ps} = 0.8793 [kJ/kg - K]$	$S_w = 20\% [vol/vol]$
$c_{pw} = 4.1868 [kJ/kg - K]$	$T_{st} = 550 K$
$h_c = 280.87 [kJ/h - m^2 - K]$	$T_i = 300 K$
$k_g = 0.0143 [kJ/h - m - K]$	$\rho_g = 16.7121 [kg/m^3]$
$k_o = 1.3962 [kJ/h - m - K]$	$\rho_o = 800.923 [kg/m^3]$
$k_s = 9.3460 [kJ/h - m - K]$	$\rho_s = 2675.08 [kg/m^3]$
$k_w = 3.7758 [kJ/h - m - K]$	$\rho_w = 1000.0 [kg/m^3]$
$k = 10^{-15} [m^2]$	$\phi = 25\% [m^3/m^3]$
$p_i = 48263299.0 [Pa]$	$\mu_f = 10 Pa.s [Ns/m^2]$
$c_f = 12.473 \times 10^{-10} [1/Pa]$	$q_i = 17.5 m^3/d [110 bbl/day]$
$c_s = 5.80147 \times 10^{-10} [1/Pa]$	$A = 300 m \times 20 m = 6000 m^2$